Abnormal photoluminescence for GaAs/$Al_{0.2}Ga_{0.8}As$ quantum dot - ring hybrid nanostructure grown by droplet epitaxy

Linlin Su[1], Baolai Liang[1, 2]*, Ying Wang[1], Qing Yuan[1], Qinglin Guo[1], Shufang Wang[1], Guangsheng Fu[1] , Diana L Huffaker[2], Yuriy I. Mazur[3], Morgan E. Ware[3], Yurii Maidaniuk[3], Gregory J. Salamo[3]

[1] *College of Physics Science & Technology, Hebei University, Baoding 071002, P.R. China*

[2] *California NanoSystem Institute, University of California - Los Angeles, CA 90095, U.S.A.*

[3] *Institute for Nanoscience and Engineering, University of Arkansas, AR 72701, U.S.A.*

*Corresponding to: liangbaolai@gmail.com

Abstract: The optical properties have been investigated for the GaAs/$Al_{0.2}Ga_{0.8}As$ quantum dot-ring hybrid nanostructures grown by droplet epitaxy, in which each nanostructure consists of four quantum dots (QDs) sitting on a distinct ring of GaAs. A blueshift and narrowing of the photoluminescence (PL) spectra along with the nonlinear decay of the time-resolved PL curves of the QDs have been observed. These abnormal PL behaviors are caused by the unique state filling effect correlated with the quantum dot-ring structure feature, which is strongly affected by carrier transfer from smaller dots to larger dots via the wetting ring in the GaAs/$Al_{0.2}Ga_{0.8}As$ hybrid structure.

Key Words: Photoluminescence, carrier dynamics, droplet epitaxy, nanostructures, semiconductor

1. Introduction

Droplet epitaxy (DE) for semiconductor nanostructures has recently attracted much attention as the DE growth mode enables flexible control of the geometry of various nanostructures and as such control of their optical and electrical properties [1-5]. In particular, DE is suitable for fabrication of novel nanostructures from not only lattice-mismatched but also lattice-matched materials [5-10]. Up to date, versatile well-defined GaAs/AlGaAs nanostructures of "zero-strain" have been fabricated by DE growth, including quantum dots (QDs), QD-pairs, QD-clusters, quantum holes, and quantum rings (QRs) [11-19]. These nanostructures have a great deal of promising advantages for optoelectronic device applications. For example, multiple stacked zero-strained GaAs/AlGaAs QD nanostructures are obtained for infrared photodetectors and photovoltaics by vertically correlated DE growth [4, 14, 20-22]. Also, a lattice-matched ring-shaped GaAs/AlGaAs laser has been reported employing DE [23].

In the DE growth of lattice-matched GaAs/AlGaAs nanostructures, the transition in geometry from dot to ring can be implemented by tailoring the substrate temperature and changing the arsenic flux, which changes the balance between crystallization inside and at the edge of the droplets [3]. In our previous study of type-I to type-II band-alignment transitions for QRs grown by DE [11], we observed that that each individual QR is not in a perfectly formed toroidal shape, but has fluctuations in height around the ring. This height fluctuation leads to special state filling effects for the QRs. In this paper we have carefully studied the optical performance and underlying mechanism of GaAs/$Al_{0.2}Ga_{0.8}As$ quantum dot-ring hybrid nanostructures with four identifiable QDs sitting on a wetting ring in each individual structure.

Abnormal luminescent behavior from these hybrid nanostructures is observed where the photoluminescence (PL) peak blueshifts and the linewidth narrows with increasing laser excitation intensity, revealing the effect of carrier transfer from smaller dots to larger dots via the wetting ring in each hybrid structure.

2. Experiments

The samples were grown by DE on semi-insulating GaAs (100) substrates in a solid source VEECO GEN-930 molecular beam epitaxy (MBE) reactor. First, a 150nm GaAs buffer and a 100nm $Al_{0.2}Ga_{0.8}As$ layer were grown at 580°C. Then, the substrate temperature was lowered from 580°C to 400°C while the As_2 flux was turned off at 500°C. The remaining As_2 in the MBE chamber was thoroughly pumped out for 5 minutes bringing the background pressure down to ~3.5E-10 Torr. After that, Ga atoms equivalent to form 6-monolayers (ML) of GaAs were deposited to obtain Ga droplets on the $Al_{0.2}Ga_{0.8}As$ surface, followed by a growth interruption of 10-seconds without As_2 flux. Then, the sample surface was exposed to an As_2 molecular beam (beam equivalent pressure = 2E-6 Torr) for 5 minutes to turn the Ga droplets into well-defined GaAs nanostructures while the substrate temperature was increased from 400°C to 500°C. The GaAs nanostructure layer was initially capped by 10nm $Al_{0.2}Ga_{0.8}As$ at 500°C and then by 90nm $Al_{0.2}Ga_{0.8}As$ at 580°C. Finally, a 3nm GaAs capping layer was grown to protect the sample surface.

The capped sample was characterized by PL and time-resolved photoluminescence (TRPL) measurements to investigate the optical properties. For reference, one sample with uncapped

GaAs nanostructures was also grown using the same conditions mentioned above for morphology study. Atomic force microscope (AFM) measurements were implemented immediately after removing the sample from the MBE growth chamber. For PL, the sample was mounted in a closed-cycle cryostat with temperature variable from 10K to 300K. The sample was excited by a continuous-wave 532nm laser and detected by a liquid nitrogen cooled CCD detector array attached to an Acton SP2500 spectrometer. For TRPL, the sample was excited by a NKT super-continuum pulse laser (λ=490nm, pulse width ~20ps, frequency 8MHz). The TRPL signal was measured by a PicoHarp-300 time-correlated-single-photon-counting (TCSPC) system with an overall system resolution of ~40ps.

3. **Results and discussion**

Figure 1(a) shows a 1μm×1μm AFM image of the uncapped GaAs/$Al_{0.2}Ga_{0.8}As$ nanostructures. In order to clearly see the morphologic features, Fig. 1(b) presents a three-dimensional (3D) projection and Fig. 1(c) gives the cross-sectional height profile of a representative nanostructure. It is clear that, after the growth, every Ga droplet has turned into a hybrid nanostructure with a hole in the center and a ring-like structure surrounding it. The general morphological characteristics of the hybrid nanostructures are similar to the undulated nano rings in our previous study [11]. The formation of GaAs hybrid nanostructures is mainly due to the migration of Ga atoms during the crystallization of Ga droplets under a suitable temperature and arsenic flux [24]. However, Ga-rich conditions result in the deep hole at the center of each hybrid nanostructure. This has been studied as a part of the DE growth mechanisms and

has been called the nano-drill effect.[25-26] The nanoholes have an average depth of ~1.8 nm measured from the sample surface. The rings have an average top diameter of ~38 nm, an outside diameter of ~64 nm, and an areal density of ~5.2×10^{9} cm^{-2}. Fig. 1(d) shows the height profile along a path around the rim of an individual ring-like structure shown by the green line in the inset. Here, it can be seen that, each ring-like structure has four QDs with the height fluctuations between 0.5nm to 0.8nm. Therefore, they are named quantum dot-ring hybrid nanostructures. It is expected that the height fluctuation of the QDs can lead to variations of the quantum confined energy levels and subsequently affect the optical performance of these GaAs/$Al_{0.2}Ga_{0.8}As$ hybrid quantum dot-ring nanostructures. This will be well demonstrated through PL measurements.

Figure 2 shows two PL spectra of the hybrid structures measured at 10 K with a weak excitation intensity of 10 mw/cm^2 and a strong excitation intensity of 3000 W/cm^2, respectively. Only one peak originating from the QDs is identified at ~758 nm (1.636 eV) under the weak excitation. But three different peaks can be observed under strong excitation. The peak at 751 nm (1.651 eV) is assigned to the QDs, and the emission around 693 nm (1.789 eV) is coming from the $Al_{0.2}Ga_{0.8}As$ barrier. The energy separation between the 751 nm (1.651 eV) and 730 nm (1.698 eV) peaks is ~47 meV, which is much larger than the typical energy separation from the ground state to the excited state of GaAs/$Al_{0.2}Ga_{0.8}As$ QDs.[27] Although it is still possible for this to be from excited states of the GaAs QDs [9], due to the large energy separation we believe that the final peak at 730 nm is from the wetting ring. The pronounced PL peak of the wetting ring under strong excitation is likely due to the relatively low density of the QDs, giving a relatively stronger PL signal for the wetting ring than the QDs [25].

In order to completely understand the mechanisms underlying the PL observations, we calculate the band profile for the GaAs/$Al_{0.2}Ga_{0.8}As$ hybrid structure using an eight-band k·p model in the Nextnano software based on the detailed structural information obtained from the AFM. The material parameters for the calculations are taken from the review in Ref. [28] and evaluated at 10K. In the calculation we neglected the strain and the small lattice-mismatch between the GaAs and the $Al_{0.2}Ga_{0.8}As$ layer. The calculated band profile of the GaAs/$Al_{0.2}Ga_{0.8}As$ hybrid structure is shown in Fig. 2(b). Figure 2(c) presents the calculated E1-H1 transition energy as a function of the height of the hybrid structure. It can be seen that the E1-H1 emission energies match with the measured PL peak energy when we take a height of ~3nm for the calculation. This indicates that the actual height of GaAs/$Al_{0.2}Ga_{0.8}As$ nanostructure formed during DE must be larger than the sum of the heights of the ring and QDs above the $Al_{0.2}Ga_{0.8}As$ surface. Therefore, we propose that there are GaAs structures on the sidewall of the nanohole similar to the inset of Fig. 2(c). With this model of the hybrid structure including the QDs, ring, and nanohole, the overall height of the GaAs/$Al_{0.2}Ga_{0.8}As$ nanostructure matches well with the 3nm determined from the simulation. The calculation also indicates the absence of excited states for the QDs, which supports the claim that the 730nm peak in Fig. 2(a) is the wetting ring emission and not from an excited state of the QDs. In consideration of the wetting ring, if we take its height as ~2.3nm (i.e., the average nanohole height of 1.8nm plus the average ring height of 0.5nm, as indicated in Fig. 1), the calculated transition energy (1.679eV) in Fig. 2(b) for wetting ring matches well with its measured, PL value (730nm, i.e., 1.698eV) in Fig. 2(a).

The PL spectra of these ring-like, hybrid structures have been investigated at 10K as a function of excitation laser intensity in Fig. 3(a). The peak position, FWHM, and integrated PL intensity are extracted and plotted in Figs. 3(b), (c), and (d), respectively. Interestingly, we notice abnormal PL behaviors from the QD PL peak. The PL peak exhibits a blueshift with an s-shaped dependence on the excitation laser intensity which is apparent already at these intensities. This peak shifts from 760 nm (1.631 eV) to 751 nm (1.651 eV) while the excitation intensity increases by six orders of magnitude from 0.003W/cm^2 to 3000 W/cm^2. Meanwhile, the linewidth decreases monotonically from 12.1 nm to 10.2 nm as the excitation intensity increases from 0.003W/cm^2 to 0.9 W/cm^2, and then the linewidth increases to 15.5 nm with the laser intensity up to 3000 W/cm^2. In addition, the integrated PL intensity linearly depends on the excitation laser intensity up to 9 W/cm^2, after which the peak from the wetting ring appears as indicated by the normalized PL spectra in Fig. 3(e).

The abnormal PL behavior is likely the result of state filling in the QDs. Indeed, with a 532nm excitation laser, the carriers are mainly generated inside the $Al_{0.2}Ga_{0.8}As$ barrier and then relax into the wetting ring and the QDs. Due to their different sizes the QDs have different probabilities to be populated by carriers. Because the wetting ring reduces the potential barrier between the QDs, there is an efficient channel for carrier transfer between them.[29] Therefore, the larger QDs have a larger carrier capture probability for weak excitation than the smaller dots. With increasing excitation intensity, the large QDs begin to saturate and the smaller QDs have an increasingly higher probability to be populated. This band filling and carrier redistribution between families of QDs results in an apparent blueshift and linewidth narrowing in the PL

spectra as the excitation intensity increases. However, as the excitation intensity increases to above 9 W/cm^2, the QDs become saturated and the wetting ring peak becomes more prominent in the spectra.

In order to further study this GaAs/$Al_{0.2}Ga_{0.8}As$ hybrid structure, PL spectra were measured as a function of temperature between 10 K and 150 K using a laser intensity of 3 W/cm^2. In this case, the QD emission is dominant in the PL spectra. As shown in Fig. 4(a), as the temperature increases the PL spectrum shifts towards longer wavelength, while the integrated PL intensity decreases. Figures 4(b), (c), and (d) present the extracted QD PL peak position, FWHM, and integrated PL intensities as functions of temperature. The QD PL peak shifts from 754.5 nm (1.643 eV) to 762.2 nm (1.627 eV), i.e., a redshift of 16 meV as the temperature increases from 10 K to 110 K. The FWHM narrows from 11.2 nm to 10.4 nm as the temperature increases from 10 K to 60 K. While, above 60 K, the PL broadens until it reaches a linewidth of 16.1 nm at 110K. The PL peak energy of the QDs is also plotted in Fig. 4(b) as a function of the temperature along with a theoretical calculation of the bandgap according to the Varshni law $E_g(T)=E_g(0)-\alpha T^2/(T+\beta)$ shown by the solid curve. Here the parameters (α=398 μeV/K, β=244K) of bulk GaAs are used [30]. Clearly, the PL peak energy of the QDs is much more sensitive than GaAs to the changes of temperature from T=20K. Such redshift of the QD PL peak energy cannot be interpreted by the temperature dependence of the semiconductor bandgap alone. The redshift combined with the FWHM narrowing from low temperature reflects the thermal excitation and redistribution of carriers between the QDs in the GaAs/$Al_{0.2}Ga_{0.8}As$ hybrid structure. Here, the height fluctuations of the ODs cause variations in the quantum confined

energy levels, and the existence of the wetting ring increases the possibility of lateral carrier transfer among the QDs. With increasing temperature, carriers are thermally excited from the higher energy, smaller QDs and transfer to the lower energy, larger QDs via the wetting ring. This effective carrier redistribution from smaller QDs to larger QDs through the ring results in a redshift and narrowing of the PL. With further increase in temperature, the effect of electron-phonon scattering becomes a dominant effect and the PL linewidth begins to increase. Finally, the PL intensity decreases with significant increase in temperature due to thermal excitation of the carriers from the QD states and subsequent transfer to nonradiative centers.

We then measured the PL spectra as a function of temperature using a strong excitation intensity of 3000 W/cm^2 to highlight the PL characteristics of the wetting ring with respect to the QDs as a function of temperature in Fig. 5(a), with the extracted peak position, FWHM, and integrated PL intensity of the wetting ring as functions of temperature in Figs. 5(b), (c), and (d), respectively. In comparison with the QD PL band, the PL linewidth of the wetting ring does not initially decrease as the temperature increases. Additionally, we find a slight increase in its integrated PL intensity in the low temperature range from 10 K to 30 K, as shown in Fig. 5(d), inset. After that it decreases monotonically up to 300 K. This supports the model of the carriers being thermally excited out of the high energy QDs, then relaxing in and contributing to the recombination in the wetting ring. To support this idea we plot the PL peak energy of the wetting ring in Fig. 5(b) as a function of the temperature, where the solid curve again is the bandgap calculated according to the Varshni law. Below 100K, the red-shift of the PL peak energy with temperature agrees very well with the change of the GaAs band gap, which means the peak shift

of the wetting ring is mainly caused by the variation of the GaAs band gap. Above 100K, however, the PL peak energy starts to depart from the calculated values. In this temperature range the carriers become thermally swept out from the wetting rings.

We also measured the time-resolved PL (TRPL) curves of the GaAs/$Al_{0.2}Ga_{0.8}As$ hybrid structure using a λ=490 nm pulsed laser with an excitation intensity of 6.1 mW. Fig. 6(a) shows the normalized TRPL curves detected at the wavelengths of the AlGaAs barrier, the QDs, and the wetting ring at 10 K. These all show an approximately mono-exponential decay behavior. The AlGaAs curve follows closely the laser pulse seen on the same plot, which means that the lifetime of carriers in the AlGaAs barrier as they decay either radiatively or through relaxation into the rings and QDs must be less than the pulse length of the laser at ~0.04ns. There is a slight delay between the maximum emission time of the AlGaAs and that of the wetting ring, which reinforces the idea that carriers are relaxing from the barrier to the ring.[11, 31] Subsequently, the decay lifetime of the PL from the wetting ring is measured to be ~0.11ns. We can see now, though, a very significant delay between the maxima of emission of the wetting rings and the QDs which is approximately the same time as the measured lifetime of the rings. This again indicates that the carriers are relaxing from the wetting rings into the QDs before recombination in the QDs and that the decay time measured for the wetting rings is dominated by this relaxation. The radiative lifetime of the QDs should be longer, which we can measure to be ~0.41ns. This agrees well with the reported lifetime of GaAs/AlGaAs QDs.[31-32]

Additionally, we measured the TRPL curves of the QDs as a function of temperature, as shown in Fig. 6(b). The maximum carrier lifetime of 0.44 ns is obtained at T=40 K, while

between 40K and 100 K the lifetime decreases down to ~0.11 ns. As the temperature increases from 10K to 40 K, the carriers can escape from smaller QDs and be captured by larger QDs through the wetting ring, giving a slightly longer lifetime measured for larger QDs. This agrees well with the variations of the integrated PL intensity and FWHM of the wetting ring shown in Fig. 4 and Fig. 5.

4. **Conclusions**

In summary, the optical properties of GaAs/$Al_{0.2}Ga_{0.8}As$ quantum dot-ring hybrid structures have been investigated via PL and TRPL measurements. First, AFM indicates that each individual hybrid nanostructure has four QDs sitting on a wetting ring. Then, a blueshift and narrowing of the spectra have been observed for QDs with increasing laser excitation intensity. In addition, the temperature-dependent PL and nonlinear decay curves show that the QDs have carrier dynamics different from the wetting ring. These abnormal PL behaviors are caused by the unique state filling effect resulting from the special quantum dot-ring structure feature, which allows for efficient carrier transfer from smaller dots to larger dots via the wetting ring in each individual GaAs/$Al_{0.2}Ga_{0.8}As$ hybrid nanostructure.

Acknowledgement: The authors acknowledge the support by the “Hebei Province 100-Talents Program” (Grant # E2013100013) of People’s Republic of China, Natural Science Foundation of People’s Republic of China (Grant#61774053), the CNSI/HP seeding funding (Grant # 449041-HD-79740), and the National Science Foundation of the US (EPSCoR Grant # OIA-1457888).

Reference：

1. N. Koguchi, S. Takahashi, T. Chikyow, New MBE growth method for InSb quantum well boxes, *Journal of Crystal Growth* 111 (1991) 688-692.
2. N. Koguchi, K. Ishige, Growth of GaAs epitaxial microcrystals on an S-terminated GaAs substrate by successive irradiation of Ga and As molecular beams, *Japanese Journal of Applied Physics* 32 (1993) 2052.
3. Z. M. Wang, K. Holmes, Yu. I. Mazur, K. A. Ramsey, and G. J. Salamo, Self-organization of quantum-dot pairs by high-temperature droplet epitaxy, *Nanoscale Research Letters* 1 (2006) 57-61.
4. J. Wu, Y. Hirono, X. Li, Z M Wang, J. H. Lee, M. Benamara, S. Luo, Yu. I. Mazur, E. S. Kim, G. J. Salamo, Self-Assembly of Multiple Stacked Nanorings by Vertically Correlated Droplet Epitaxy, *Advanced Functional Materials* 24 (2014) 530-535.
5. M. Takaaki, K. Takashi, S. Stefano, O. Tetsuyuki, T. Takahiro, K. Jongsu, N. Takeshi, K. Mitsuo, S. Kazuaki, K. Giyuu, K. Nobuyuki, Self-assembly of concentric quantum double rings, *Nano Letters* 5 (2005) 425-428.
6. K. A. Sablon, Zh. M. Wang, G. J. Salamo, Composite droplets: evolution of InGa and AlGa alloys on GaAs(100), *Nanotechnology* 19 (2008) 125609.
7. C. Heyn, A. Stemmann, T. Koppen, C. Strelow, T. Kipp, M. Grave, Highly uniform and strain-free GaAs quantum dots fabricated by filling of self-assembled nanoholes, *Applied Physics Letters* 94 (2009) 183113.
8. A. Z. Li, Z. M. Wang, J. Wu, Y. Xie, K. A. Sablon, G. J. Salamo, Evolution of Holed

Nanostructures on GaAs (001), *Crystal Growth & Design* 9 (2009) 2941-2943.

9. C. Z. Tong, and S. F. Yoon, Investigation of the fabrication mechanism of self-assembled GaAs quantum rings grown by droplet epitaxy, *Nanotechnology* 19 (2008) 365604.

10. C. Somaschini, S. Bietti, N. Koguchi, S. Sanguinetti, Coupled quantum dot–ring structures by droplet epitaxy, *Nanotechnology* 22 (2011) 185602.

11. L. L. Su, Y. Wang, Q. L. Guo, S. F. Wang, G. S. Fu, Yu. I. Mazur, M. E. Ware, G. J. Salamo, B. L. Liang, D. L. Huffaker, Optical Characterization of Type-I to Type-II Band Alignment Transition in GaAs/AlxGa1-xAs quantum rings grown by droplet epitaxy, *J Physics D: Applied Physics* 50 (2017) 32LT01.

12. T. Mano, N Koguchi, Nanometer-scale GaAs ring structure grown by droplet epitaxy, *Journal of Crystal Growth* 278 (2005) 108-112.

13. Z. M. Wang, B. L. Liang, K. A. Sablon, J. H. Lee, Yu. I. Mazur, N. W. Strom, G. J. Salamo. Self-organization of InAs quantum-dot clusters directed by droplet homoepitaxy, *Small* 3 (2007) 235-238.

14. J. Wu, D. Shao, V. G. Dorogan, A. Z. Li, S. Li, E. A. DeCuir, M. O. Manasreh, Z. M. Wang, Yu. I. Mazur, G. J. Salamo, Intersublevel infrared photodetector with strain-free GaAs quantum dot pairs grown by high-temperature droplet epitaxy, *Nano Letters* 10(2010) 1512-1516.

15. T. Kuroda, T. Mano, T. Ochiai, S. Sanguinetti, K. Sakoda, G. Kido, N Koguchi, Optical transitions in quantum ring complexes, *Physical Review B* 72 (2005) 205301.

16. A. Scaccabarozzi, S. Adorno, S. Bietti, M. Acciarri, S. Sanguinetti, Evidence of two-photon absorption in strain-free quantum dot GaAs/AlGaAs solar cells, *Phys. Status Solidi RRL* 7 (2013) 173–176
17. K. Watanabe, N. Koguchi, Y Gotoh, Fabrication of GaAs Quantum Dots by Modified Droplet Epitaxy, *Japanese Journal of Applied Physics* 39(2000) L79-L81.
18. D. Granados, J. M. García, In(Ga)As self-assembled quantum ring formation by molecular beam epitaxy, *Applied Physics Letters* 82 (2003) 2401-2403.
19. C. H. Lin, H. S. Lin, C. C. Huang, S. K. Su, S. D. Lin, K. W. Sun, C. P. Lee, Y. K. Liu, M. D. Yang, and J. L. Shen. Temperature dependence of time-resolved photoluminescence spectroscopy in InAs/GaAs quantum ring, *Applied Physics Letters* 94(2009) 183101.
20. J. Wu, Z. Li, D. Shao, M. O. Manasreh, V. P. Kunets, Z. M. Wang, B. D. Weaver, Multicolor photodetector based on GaAs quantum rings grown by droplet epitaxy, *Applied Physics Letters* 94 (2009) 171102.
21. P. Yu, J. Wu, L. Gao, H. Y. Liu, Z. M. Wang, InGaAs and GaAs quantum dot solar cells grown by droplet epitaxy, *Solar Energy Materials and Solar Cells* 161 (2017) 377-381.
22. A. Scaccabarozzi, S. Adorno, S. Bietti, M. Acciarri, S. Sanguinetti, Evidence of two photon absorption in strain-free quantum dot GaAs/AlGaAs solar cells, *Physica Status Solidi (RRL) – Rapid Res. Lett.* 7 (2013) 173–176.
23. T. Mano, T. Kuroda, K. Mitsuishi, M. Yamagiwa, X. J. Guo, K. Furuya, K. Sakodaa, N Koguchi, Ring-shaped GaAs quantum dot laser grown by droplet epitaxy: effects of post-growth annealing on structural and optical properties, *Journal of Crystal Growth* 301

(2007) 740-743.

24. S. Bietti, C. Somaschini, S. Sanguinetti, Crystallization kinetics of Ga metallic nano-droplets under As flux, *Nanotechnology* 24 (2013) 205603

25. B. L. Liang, Z. M. Wang, J. H. Lee, K. A. Sablon, Yu. I. Mazur, G. J.Salamo. Low density InAs quantum dots grown on GaAs nanoholes, *Applied Physics Letters* 89 (2006) 043113.

26. Zh. M. Wang, B. L. Liang, K. A. Sablon, G. J. Salamo, Nanoholes fabricated by self-assembled nano drill on GaAs(100), *Appl. Phys Lett*. 90(2007) 113120.

27. A. Rastelli, S. Stufler, A. Schliwa, R. Songmuang, C. Manzano, G. Costantini, K. Kern, A. Zrenner, D. Bimberg, O. G. Schmidt, Hierarchical self-assembly of GaAs/AlGaAs quantum dots, *Physical Review Letters* 92 (2004) 166104.

28. I. Vurgaftman, J. R. Meyer, L. R. Ram-Mohan, Band parameters for III–V compound semiconductors and their alloys, *J. Appl. Phys*. 89 (2001) 5815-5875.

29. B. L. Liang, Z. M. Wang, X. Y. Wang, J. H. Lee, Yu. I. Mazur, C. K. Shih, G. J. Salamo, Energy transfer within ultralow density twin InAs quantum dots grown by droplet epitaxy, *Acs Nano* 2 (2008) 2219-2224.

30. K. P. O'Donnell, and X. Chen, Temperature dependence of semiconductor band gaps, *Appl. Phys. Lett.* 58, (1991) 2924-2926

31. K. Kuroda, T. Kuroda, K. Watanabe, T. Mano, G. Kido, N. Koguchi, K. Sakoda, Distribution of exciton emission linewidth observed for GaAs quantum dots grown by droplet epitaxy, *Journal of Luminescence*, 130 (2010) 2390-2393.

32. J. Kim, H. Kang, C. C. Byeon, M. Jeong, S. Y. Yim, J. Kim, S. Lee, S. Noh, J. Kim, J. Y.

Leem, Size dependence of the photoluminescence decay time in unstrained GaAs quantum dots, *Journal of Korean Physical Society* 55 (2009) 1051-1055 (DOI: 10.3938/jkps.55.1051).

Captions

Figure 1. AFM image and morphological property analysis of the GaAs/$Al_{0.2}Ga_{0.8}As$ hybrid nanostructures. (a) 1μm×1μm AFM image; (b) 3D projection to show two individual nanostructures; (c) The cross-section profile of one nanostructure; (d) height fluctuation of an individual ring-like nanostructure along a path shown by the green line on the top of the nanostructure shown in the inset.

Figure 2. (a) PL spectra of GaAs/$Al_{0.2}Ga_{0.8}As$ hybrid nanostructures measured at T=10 K with a weak excitation intensity of 10 mW/cm^2 and a strong excitation intensity of 3000 W/cm^2, respectively, (b) Calculated band profile diagram for the GaAs/$Al_{0.2}Ga_{0.8}As$ hybrid nanostructures; (c) calculated E1-H1 transition energy as a function of the height of the hybrid nanostructure.

Figure 3. (a) PL spectra of GaAs/$Al_{0.2}Ga_{0.8}As$ hybrid nanostructures are measured at T=10K as a function of the laser excitation intensity. The peak position (b), FWHM (c), and integrated intensity (d) of the QDs extracted as functions of the laser excitation intensity, (e) normalized, linear plots of the QD spectra for laser excitation intensities covering three orders of magnitude from 0.03W/cm^2 to 30 W/cm^2..

Figure 4. (a) Temperature-dependent PL spectra of GaAs/$Al_{0.2}Ga_{0.8}As$ hybrid nanostructures measured at an excitation laser intensity of 3 mW/cm^2; The peak position (b), FWHM (c), and PL integrated intensity (d) of QD peak are plotted as a function of temperature.

Figure 5. (a) Temperature-dependent PL spectra of GaAs/$Al_{0.2}Ga_{0.8}As$ hybrid nanostructures measured at an excitation laser intensity of 3000 mW/cm^2; The peak position (b), FWHM (c), and integrated intensity (d) of the wetting ring peak are extracted as a function of the temperature

Figure 6. (a) The TRPL curves at T=10 K for GaAs/$Al_{0.2}Ga_{0.8}As$ QRs detected at different peak position with the laser excitation intensity of 6.1 mW; (b) carrier lifetime of the QDs as a function of temperature.

Figure 1. AFM image and morphological property analysis of the GaAs/$Al_{0.2}Ga_{0.8}As$ hybrid nanostructures. (a) 1μm×1μm AFM image; (b) 3D projection to show two individual nanostructures; (c) The cross-section profile of one nanostructure; (d) height fluctuation of an individual ring-like nanostructure along a path shown by the green line on the top of the nanostructure shown in the inset.

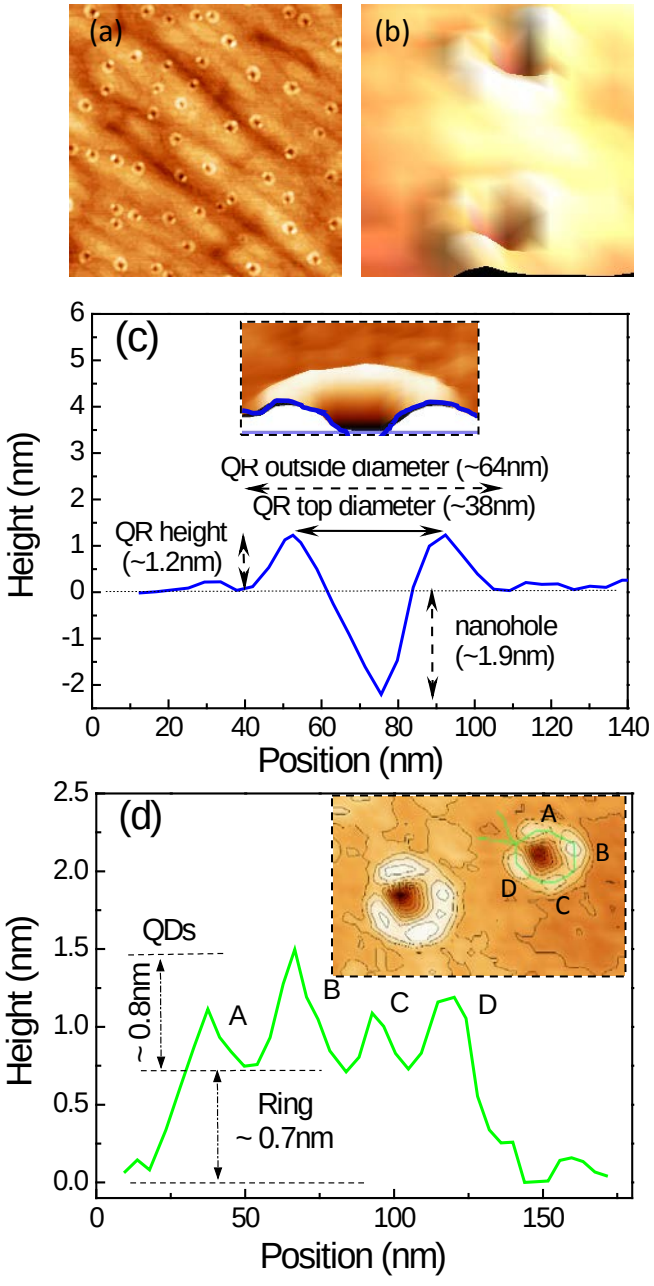

Figure 2. (a) PL spectra of GaAs/$Al_{0.2}Ga_{0.8}As$ hybrid nanostructures measured at T=10 K with a weak excitation intensity of 10 mW/cm^2 and a strong excitation intensity of 3000 W/cm^2, respectively, (b) Calculated band profile diagram for the GaAs/$Al_{0.2}Ga_{0.8}As$ hybrid nanostructures; (c) calculated E1-H1 transition energy as a function of the height of the hybrid nanostructure.

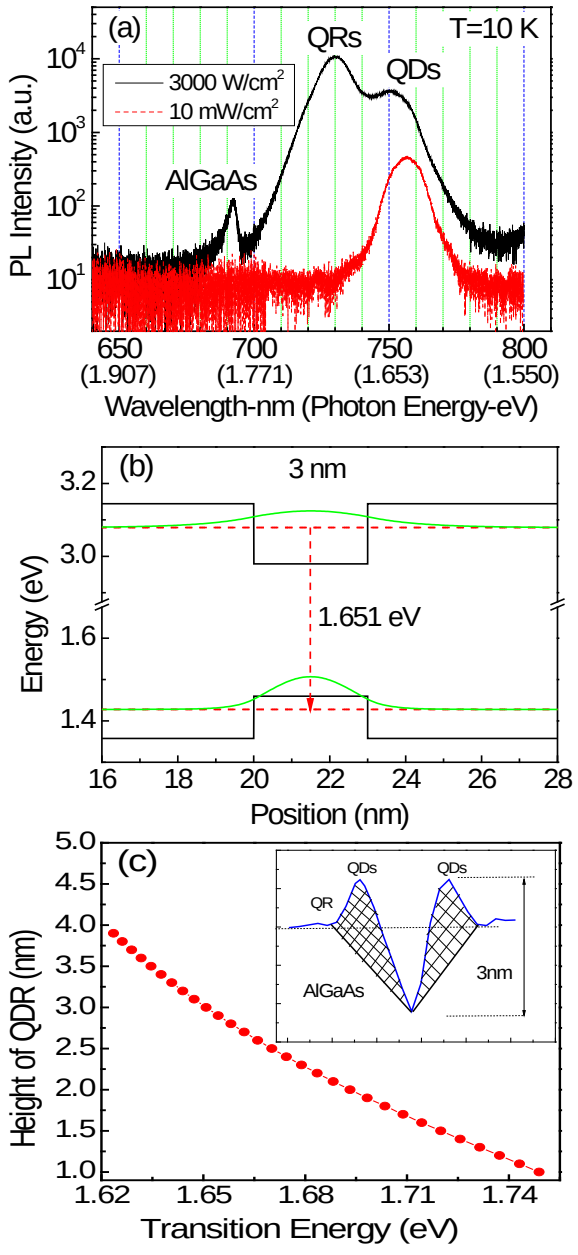

Figure 3. (a) PL spectra of GaAs/$Al_{0.2}Ga_{0.8}As$ hybrid nanostructures are measured at T=10K as a function of the laser excitation intensity. The peak position (b), FWHM (c), and integrated intensity (d) of the QDs extracted as functions of the laser excitation intensity, (e) normalized, linear plots of the QD spectra for laser excitation intensities covering three orders of magnitude from 0.03W/cm^2 to 30 W/cm^2.

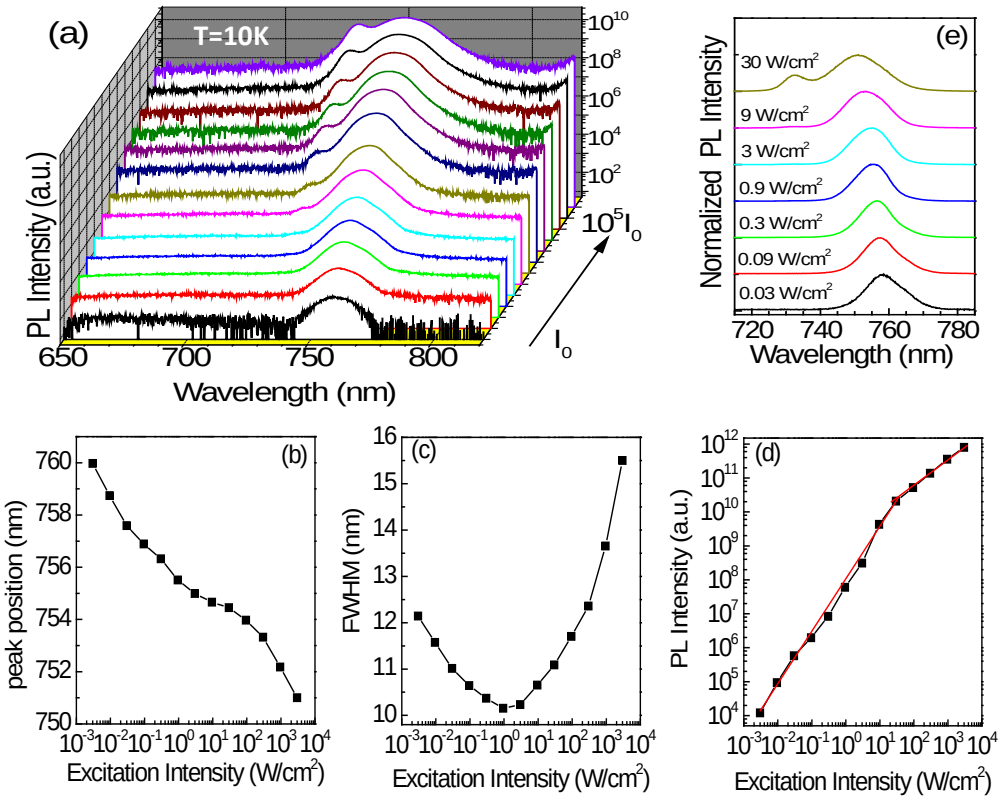

Figure 4. (a) Temperature-dependent PL spectra of GaAs/$Al_{0.2}Ga_{0.8}As$ hybrid nanostructures measured at an excitation laser intensity of 3 W/cm^2; The peak position (b), FWHM (c), and PL integrated intensity (d) of QD peak are plotted as a function of temperature.

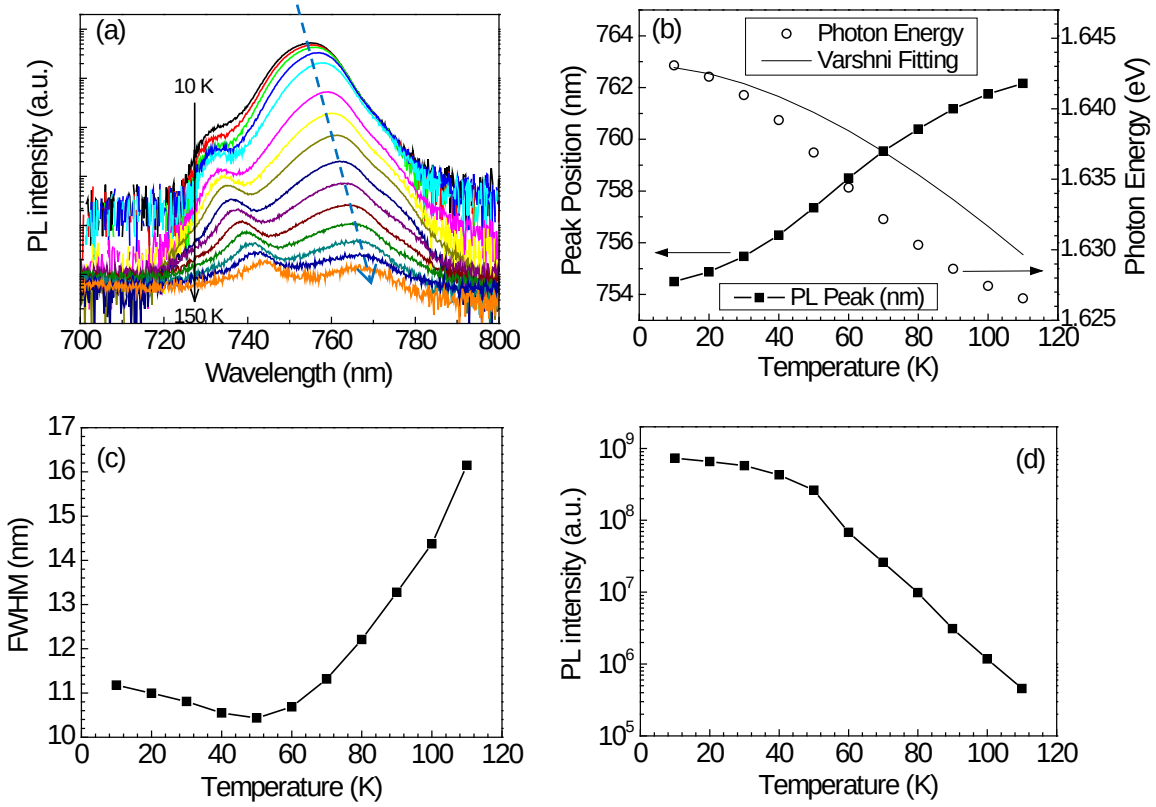

Figure 5. (a) Temperature-dependent PL spectra of GaAs/$Al_{0.2}Ga_{0.8}As$ hybrid nanostructures measured at an excitation laser intensity of 3000 W/cm^2; The peak position (b), FWHM (c), and integrated intensity (d) of the wetting ring peak are extracted as a function of the temperature

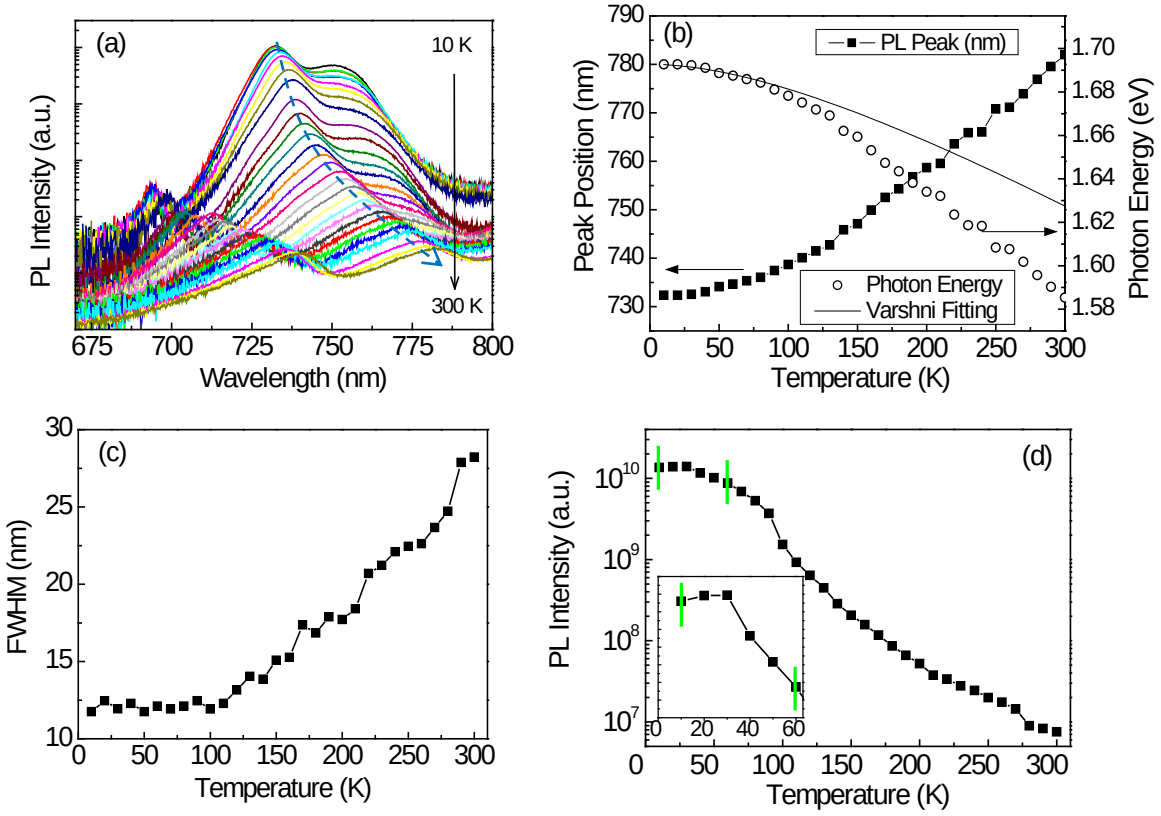

Figure 6. (a) The TRPL curves at T=10 K for GaAs/$Al_{0.2}Ga_{0.8}As$ QRs detected at different peak position with the laser excitation intensity of 6.1 mW; (b) carrier lifetime of the QDs as a function of temperature.